Supplementary material: Thermodynamic equilibrium conditions in the growth of graphene films on SiC

Lydia Nemec, Volker Blum, Patrick Rinke, and Matthias Scheffler
Fritz-Haber-Institut der Max-Planck-Gesellschaft, D-14195, Berlin, Germany
(Dated: April 29, 2013)

We describe the computational details and numerical convergence of our calculations of the SiC(111) (Si-side) surface phase diagram and structures, especially of the graphene-like reconstructed $(6\sqrt{3}\times6\sqrt{3})$R30° SiC surface phases. Calculated reference data for the bulk phases 3C-SiC, graphite and diamond are given for different functionals.

Methodology

We assess the surface phase diagram in the framework of first-principles thermodynamics, using a grand canonical formalism to compare surface energies according to Eqs. (1-3) in our paper. As first-principles input, we require accurately converged total energies for slab calculations, as well as bulk reference total energies for Si, SiC and the bulk phases of carbon, graphite and diamond.

All total energies are obtained by numerically and basis-set converged first-principles calculations using the FHI-aims all-electron code[1, 2] and the massively parallel eigenvalue solver library ELPA[3] for the solution of the Kohn-Sham equations. The density functionals used are the local-density approximation (LDA) in the parameterization by Perdew and Wang 1992[4], the generalized gradient functional PBE, [5] and PBE+vdW approach as defined by Tkatchenko and Scheffler 2009[6]. In this method, the vdW terms are included as a C_6/R^6-type sum of interatomic interactions and the C_6 coefficients are derived from the self-consistent electron density in a non-empirical way.

In our paper, we restrict ourselves to the original method proposed by Tkatchenko and Scheffler.[6] While various refinements of this scheme are under active development, to our knowledge there is no single scheme yet that would address the complex surface structures encountered in our work. For semiconductor bulk phases, however, we can compare to results from Zhang and coworkers, who showed that the C_6 dispersion coefficients are reduced compared to the free-atom values due to long-range electrostatic screening.[7] We reference to their result for 3C-SiC below.

We do not include the effects of zero-point corrections (or, indeed, of finite-temperature anharmonic effects) in any of the results presented in the main part of our paper. The reason is that the computation of the phonon dispersion necessary for such corrections for the most interesting large-scale reconstructed graphene phases would be prohibitive even on the most advanced massively parallel computer hardware available to us today (hardware used: Intel Westmere processor architecture with up to ≈1,000 CPU cores for routine production runs). However, we show below by exemplary results for the bulk phases that zero-point effects on their structure would be small.

3C-SiC bulk structure and total energies

The lattice parameter for the 3C-SiC polytype used in this work are listed in Table (I). For different functionals the lattice parameter shows variations of the order of 1 % at most. The zero-T extrapolated experimental value is 4.36 Å.[8] The PBE+vdW method employed in this work comes very close to this result, both for results calculated at the bare potential energy surface, or with zero-point corrections (ZPC) included in the quasi-harmonic approximation.

Zero-point corrections for 3C-SiC were evaluated by full phonon calculations in a finite-difference approach, using a $5\times5\times5$ supercell for 5 lattice parameters. The minimum-energy lattice parameter for T=0 K was obtained by fitting to the Birch-Murnaghan equation of state. The inclusion of zero-point corrections results only in small changes of the bullk cohesive properties.

The lattice parameter obtained from a refined van der Waals treatment for the 3C SiC bulk phase, obtained by Zhang *et al.*,[7] is also given in Table I. The effect on the structure is small.

Elemental phases: diamond, graphite and silicon

The lattice parameter for the reference bulk systems C-diamond, graphite and silicon used in this work are listed in Table (II) for different functionals. The impact of zero-point corrections (ZPC) is similarly small as for 3C-SiC. For the interplanar lattice parameter c of graphite, vdW effects must be included into the PBE functional.

3C SiC: Enthalpy of formation

The enthalpy of formation ΔH_f is calculated for bulk silicon and carbon in the diamond structure as the reference phases. ΔH_f is between -0.53 eV and -0.56 eV, depending on the density-functional used, and shows good

	PBE+vdW		PBE		LDA		PBE+vdW^{scr}	experiment
	PES	ZPC	PES	ZPC	PES	ZPC	PES	
a_0 [Å]	4.36	4.38	4.38	4.40	4.33	4.34	4.38	4.36 [8]
B_0 [Mbar]	2.10	2.09	2.10	2.06	2.30	2.23	2.12	
e_{coh} [eV]	-6.76	-6.65	-6.52	-6.41	-7.41	-7.30		
ΔH_f [eV]	-0.56		-0.53		-0.56			

TABLE I: For 3C-SiC, the lattice parameters a_0 [Å], bulk modulus B_0 [Mbar], cohesive energy e_{coh} [eV] and enthalpy of formation ΔH_f [eV] as obtained in this work. "PES" refers to results computed based on the Born-Oppenheimer potential energy surface without any corrections. Zero-point vibrational corrected (ZPC) lattice parameters and bulk moduli are given for the LDA, PBE and PBE+vdW functionals.

	PBE+vdW		PBE	LDA	
	PES	ZPC	PES	PES	ZPC
diamond a_0 [Å]	3.55	3.57	3.57	3.53	3.55
graphite a_0, c_0 [Å]	2.46, 6.66	2.47, 6.69	2.47, 8.65	2.45, 6.65	2.45, 6.66
Silicon a_0 [Å]	5.45		5.47	5.40	

TABLE II: Lattice parameter a_0 and c_0 for graphite, diamond and silicon in diamond structure as obtained in this work. "PES" refers to results computed based on the Born-Oppenheimer potential energy surface without any corrections. Zero-point vibrational corrected (ZPC) lattice parameters are given for the LDA, PBE and PBE+vdW functionals.

agreement with a calculated literature value of -0.58 eV using the pseudopotential plane wave (PSP-PW) method in the LDA [9]. The calculated cohesive energy is noteably smaller (less energy gain) than the experimental room temperature value obtained by an electromotive force (emf) measurement.[10]

Numerical convergence

Basis set

The FHI-aims code employs numeric atom-centered basis sets; basic descriptions of their mathematical form and properties are published in Ref. [2] (note that this reference is available as an open-access publication). What is important for the present purposes is to demonstrate the accurate convergence, up to a few meV at most, of our calculated surface energies with respect to the basis set used.

The FHI-aims basis sets are defined by numerically determined radial functions corresponding to different angula momentum channels. As is typical of atom-centered basis sets (Gaussian-type, Slater-type, numerically tabulated etc.), variational flexibility is achieved by successively adding radial functions for individual angular momentum channels, until convergence is achieved. In practice, the basis functions for individual elements in FHI-aims are grouped in so-called "tiers" or "levels": *tier 1*, *tier 2*, and so forth. In the present paper, basis functions for Si and C up to *tier 2* were used. The pertinent radial functions are summarized in Table (III), using the exact same notation that was established in Ref. [2].

	C	Si
minimal	[He]+2s2p	[Ne]+3s3p
tier 1	H(2p, 1.7)	H(3d, 4.2)
	H(3d, 6.0)	H(2p, 1.4)
	H(2s,4.9)	H(4f, 6.2)
		Si^{2+}(3s)
tier 2	H(4f, 9.8)	H(3d, 9.0)
	H(3p, 5.2)	H(5g, 9.4)
	H(3s, 4.3)	H(4p, 4.0)
	H(5g, 14.4)	H(1s, 0.65)
	H(3d, 6.2)	
	...	...

TABLE III: Radial functions used for C and Si. The first line ("minimal") denotes the radial functions of the occupied orbitals of spherically symmetric free atoms as computed in DFT-LDA or -PBE (noble-gas configuration of the core and quantum numbers of the additional valence radial functions). "H(nl, z)" denotes a hydrogen-like basis function for the bare Coulomb potential z/r, including its radial and angular momentum quantum numbers, n and l. X^{2+}(nl) denotes a n, l radial function of a doubly positive free ion of element X. See also Ref. [2] for notational details.

The convergence of the calculated surface energies in our paper with basis size is exemplified for the $(\sqrt{3} \times \sqrt{3})$-R30° small unit cell approximant[11, 12] to the ZLG phase in Fig. (1) including 6 SiC-bilayer. The bottom carbon atoms were saturated by hydrogen. Its geometry was first fully relaxed with FHI-aims *tight* grid settings, a *tier 1+dg* basis set for Si and a *tier 2* basis set for C basis settings. This geometry was then kept fixed for the convergence tests shown here. What is shown in Fig. (1) is the development of the surface energy (Si face and H-terminated C-face) with increasing basis size for both C and Si were calculated using

$$\gamma_{\text{Si-face}} + \gamma_{\text{C-face}} = \frac{1}{A}\left(E^{\text{slab}} - N_{\text{Si}}\mu_{\text{Si}} - N_{\text{C}}\mu_{\text{C}}\right) . \quad (1)$$

where N_{Si} and N_{C} denote the number of Si and C atoms

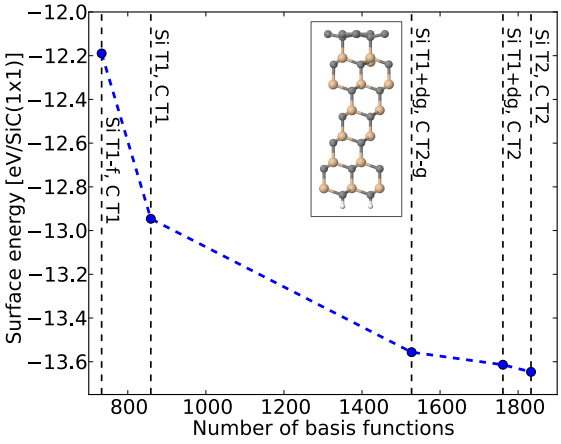

FIG. 1: Effect of increasing the basis set size on the surface energy of the $\sqrt{3}$ approximant to the ZLG phase at the chemical potential limit of bulk graphite. The PBE+vdW functional was used. In the plot we use T1 (T2) as abbrevation of *tier 1* (*tier 2*) , respectively

in the slab, respectively, and A is the chosen area. The computed surface energy is shown per 1×1 surface area as in all surface energies given in the main text.

The notation in the figure is as follows:

- "T1" and "T2" abbreviate the set of radial functions included in *tier 1* and *tier 2*, respectively (see Table III).
- "Si T1-f" denotes the Si *tier 1* basis set, but with the f radial function omitted.
- "C T2-g denotes the set of radial functions for C up to *tier 2*, but omitting the g-type radial function of *tier 2*.
- "Si T1+dg" denotes the radial functions included up to *tier 1* of Si, and additionally the d and g radial functions that are part of *tier 2*. This is also the predefined default basis set for FHI-aims "tight" settings for Si.
- "C T2" denotes the radial functions of C up to *tier 2* and is the default choice for "tight" settings in FHI-aims.

In short, the plot indicates the required convergence of the surface energy to a few meV/(1×1) surface area if the default FHI-aims "tight" settings are used. It is evident that the high-l g-type component for C contributes noticeably to the surface energy.

Slab Thickness

The convergence of our surface calculations with respect to the number of SiC bilayers is shown in Fig. (2) by considering surface energies for the $(\sqrt{3} \times \sqrt{3})$-R30° small unit cell approximant[11, 12]. The zero reference energy is an unreconstructed six bilayer 1x1 SiC surface. A six bilayer slab is sufficient to accurately represent bulk effects.

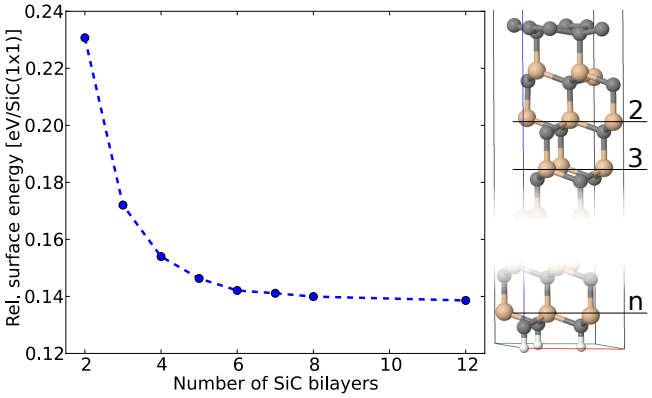

FIG. 2: Slab thickness dependence of the surface energy of the $(\sqrt{3} \times \sqrt{3})$-R30° approximant to the ZLG phase.

k-Space Integration Grids

We demonstrate the accuracy of the 2D Brillouin zone integrals for our graphene-like surface phases by comparing different k-space integration grids in Table (IV) The ZLG and MLG surface energies in the full $(6\sqrt{3}\times6\sqrt{3})$-R30° cell are compared using the Γ-point only and using a 2x2x1 k-space grid. These k-mesh tests were performed in a four bilayer slab, using the PBE+vdW functional, *light* real space integration grids, a *tier1* basis set without the f functions for Si and *tier1* for C. The geometries were kept fixed at the configuration relaxed with a Γ-point only k-space grid. In Table (IV), the surface energies relative to the unreconstructed 1x1 surface in the graphite limit are listed for the silicon rich $\sqrt{3}$x$\sqrt{3}$ reconstruction, the ZLG and MLG phases. Table (IV) clearly shows that the surface energies are well converged using the Γ-point only. Hence in this work, all surface energies for the $(6\sqrt{3}\times6\sqrt{3})$-R30° phases were calculated using this k-space integration grid. For all bulk reference energies as well as for the two silicon rich surface reconstructions, the convergence with respect to the k-mesh size has been tested and found to be well converged for grids equivalent to the ZLG phase.

system	k-grid		
	6x6x1	12x12x1	24x24x1
$\sqrt{3}$x$\sqrt{3}$	-0.439	-0.435	-0.436
	1x1x1	2x2x1	
ZLG	-0.426	-0.426	
MLG	-0.454	-0.455	

TABLE IV: Surface energies in [eV/SiC(1x1)] relative to the unreconstructed 3C-SiC(1x1) surface for the chemical potential limit of graphite, four-bilayer SiC slabs. The silicon-rich $\sqrt{3}$x$\sqrt{3}$ reconstruction, ZLG and MLG phases using different k-grids are shown. The PBE+vdW exchange-correlation functional was used.

Strategy for structure optimization

For all surface energies presented in the main text, we used a two step procedure for computationally efficient structure optimization. The first step was a prerelaxation with four bilayer SiC slabs and the additional atoms of the selected surface phase. The bottom two bilayers as well as the bottom hydrogen atoms were kept fixed, while the rest was relaxed (residual forces $< 0.8 \times 10^{-2} eV/\text{Å}$) using light real space integration grids, Si *tier* 1-f and C *tier* 1 basis sets. The second step built on the prerelaxed structures. Two additional SiC bilayers were added to the bottom of the slab. The C-side was saturated with hydrogen atoms as before. For the postrelaxation, tight integration grids, Si *tier* 1+dg and C *tier* 2 basis sets were used, while the hydrogen layer and the 3 bottom SiC layer were constrained to their bulk positions.

The hexagon-pentagon-heptagon (H5,6,7) defect in the zero-layer graphene

We consider a specific class of C-rich defects suggested as an equilibrium feature of the ZLG phase in Ref. [13]. The defects consists of three carbon heptagons and pentagons surrounding one carbon hexagon. The central hexagon is rotated by 30° with respect to the graphene lattice. This defect incoporates two additional carbon atoms lowering the average C-C bond length in the ZLG. Two different defect positions, "hollow" and "top" were suggested.[13]. In fig. (3) the H(5,6,7) defect is shown for both positions in the approximated 3×3 and in the $\left(6\sqrt{3} \times 6\sqrt{3}\right)$R30° ZLG phase. All four phases were fully relaxed using the same procedure as described above. The 3×3 is a supercell of the approximated $(\sqrt{3} \times \sqrt{3})$-R30° ZLG phase with a massively strained ($\sim 10\%$) carbon layer.

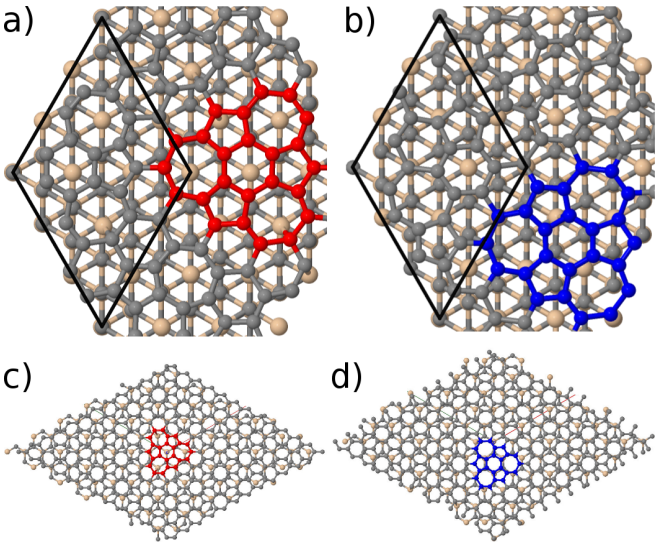

FIG. 3: The hexagon-pentagon-heptagon (H5,6,7) defect in the zero-layer graphene shown in the approximated 3×3 cell (insert a and b) and in the $\left(6\sqrt{3} \times 6\sqrt{3}\right)$R30° ZLG phase. The defect was placed in two different positions. In inset a and c the defect is placed at "hollow" position with an silicon atom of the underlying SiC bilayer in the middle of the central hexagon and at "top" position.

[1] V. Havu, V. Blum, P. Havu, and M. Scheffler, J. Comp. Phys. **228**, 8367 (2009).

[2] V. Blum, R. Gehrke, F. Hanke, P. Havu, V. Havu, X. Ren, K. Reuter, and M. Scheffler, Comp. Phys. Commun. **180**, 2175 (2009).

[3] T. Auckenthaler, V. Blum, H. Bungartz, T. Huckle, R. Johanni, L. Krämer, B. Lang, H. Lederer, and P. Willems, Parallel Computing **37**, 783 (2011).

[4] J. P. Perdew and Y. Wang, Phys. Rev. B **45**, 13244 (1992).

[5] J. P. Perdew, K. Burke, and M. Ernzerhof, Phys. Rev. Lett. **78**, 1396 (1997).

[6] A. Tkatchenko and M. Scheffler, Phys. Rev. Lett. **102**, 073005 (2009).

[7] G.-X. Zhang, A. Tkatchenko, J. Paier, H. Appel, and M. Scheffler, Phys. Rev. Lett. **107**, 245501 (2011).

[8] Z. Li and R. C. Bradt, J. Mat. Sci. **21**, 4366 (1986).

[9] A. Zywietz, J. Furthmüller, and F. Bechstedt, Physical Review B **59**, 15166 (1999).

[10] H. Kleykamp, Ber. Bunsenges. phys. Chem. **102**, 1231 (1998).

[11] F. Varchon, R. Feng, J. Hass, X. Li, B. Nguyen, C. Naud, P. Mallet, J. Veuillen, C. Berger, E. Conrad, et al., Phys. Rev. Lett. **99**, 126805 (2007).

[12] A. Mattausch and O. Pankratov, Phys. Rev. Lett. **99**, 76802 (2007).

[13] Y. Qi, S. Rhim, G. Sun, M. Weinert, and L. Li, Phys. Rev. Lett. **105**, 085502 (2010).